

Decoding fMRI events in Sensorimotor Motor Network using Sparse Paradigm Free Mapping and Activation Likelihood Estimates

Tan, Francisca M.; Mullinger, Karen

DOI:
[10.1002/hbm.23767](https://doi.org/10.1002/hbm.23767)

License:
None: All rights reserved

Document Version
Peer reviewed version

Citation for published version (Harvard):
Tan, FM & Mullinger, K 2017, 'Decoding fMRI events in Sensorimotor Motor Network using Sparse Paradigm Free Mapping and Activation Likelihood Estimates', *Human Brain Mapping*, vol. 38, no. 11, pp. 5778-5794.
<https://doi.org/10.1002/hbm.23767>

[Link to publication on Research at Birmingham portal](#)

General rights

Unless a licence is specified above, all rights (including copyright and moral rights) in this document are retained by the authors and/or the copyright holders. The express permission of the copyright holder must be obtained for any use of this material other than for purposes permitted by law.

- Users may freely distribute the URL that is used to identify this publication.
- Users may download and/or print one copy of the publication from the University of Birmingham research portal for the purpose of private study or non-commercial research.
- User may use extracts from the document in line with the concept of 'fair dealing' under the Copyright, Designs and Patents Act 1988 (?)
- Users may not further distribute the material nor use it for the purposes of commercial gain.

Where a licence is displayed above, please note the terms and conditions of the licence govern your use of this document.

When citing, please reference the published version.

Take down policy

While the University of Birmingham exercises care and attention in making items available there are rare occasions when an item has been uploaded in error or has been deemed to be commercially or otherwise sensitive.

If you believe that this is the case for this document, please contact UBIRA@lists.bham.ac.uk providing details and we will remove access to the work immediately and investigate.

Decoding fMRI events in Sensorimotor Motor Network using Sparse Paradigm Free Mapping and Activation Likelihood Estimates

Francisca M. Tan^{a,b}, César Caballero-Gaudes^c, Karen J. Mullinger^{a,e}, Siu-Yeung Cho^b, Yaping Zhang^b, Ian L. Dryden^d, Susan T. Francis^a and Penny A. Gowland^a

^a Sir Peter Mansfield Imaging Centre, School of Physics and Astronomy and School of Mathematical Sciences, ^d The University of Nottingham, University Park, Nottingham, NG7 2RD, United Kingdom

^b Department of Electrical and Electronic Engineering, University of Nottingham Ningbo China, Ningbo, 315100, People's Republic of China

^c Basque Center of Cognition, Brain and Language, San Sebastian, 20009, Spain

^e Birmingham University Imaging Centre, School of Psychology, University of Birmingham, Birmingham, B15 2TT, United Kingdom

ABSTRACT

Most fMRI studies map task-driven brain activity using a block or event-related paradigm. Sparse Paradigm Free Mapping (SPFM) can detect the onset and spatial distribution of BOLD events in the brain without prior timing information; but relating the detected events to brain function remains a challenge. In this study, we developed a decoding method for SPFM using a coordinate-based meta-analysis method of Activation Likelihood Estimation (ALE). **We defined meta-maps of statistically significant ALE values that correspond to types of events and calculated a summation overlap between the normalized meta-maps and SPFM maps. As a proof of concept, this framework was applied to relate SPFM-detected events in the Sensorimotor Network (SMN) to six motor function (left/right fingers, left/right toes, swallowing and eye blinks). We validated the framework using simultaneous Electromyography-fMRI experiments and motor tasks with short and long duration, and random inter-stimulus interval.** The decoding scores were considerably lower for eye movements relative to other movement types tested. The average successful rate for short and long motor events was $77 \pm 13\%$ and $74 \pm 16\%$ respectively, excluding eye movements. We found good agreement between the decoding results and EMG for most events and subjects, with a range in sensitivity between 55 and 100%, excluding eye movements. The proposed method was then used to classify the movement types of spontaneous single-trial events in the SMN during resting state, **which produced an average successful rate of $22 \pm 12\%$. Finally, this paper discusses methodological implications and improvements to increase the decoding performance.**

Keywords: Functional MRI, decoding, meta-analysis, Activation Likelihood Estimation, Paradigm Free Mapping.

INTRODUCTION

Resting state functional MRI (fMRI) data has been shown to contain signatures of brain activation relating to 'spontaneous events' or uncued tasks performed by the subject and recently various techniques have been developed to detect these activations (Liu et al., 2013, Smith et al., 2012, Gaudes et al., 2011, Petridou et al., 2013, Caballero Gaudes et al., 2013, Karahanoglu et al., 2013, Cisler et al., 2014, Chen et al., 2015, Allan et al., 2015). It remains a major challenge to interpret spontaneous events in terms of brain function. Brain decoding enables us to relate detected brain activity to a specific mental state (Tong and Pratte, 2012). In recent years, machine learning algorithms have been applied to fMRI brain decoding (O'Toole et al., 2005, O'Craven and Kanwisher, 2000, Haxby et al., 2001, Cox and Savoy, 2003, Haynes and Rees, 2005, Kamitani and Tong, 2005, Horikawa et al., 2013, Schrouff et al., 2012b). However, such algorithms typically require the acquisition of a training dataset involving similar experimental conditions to those that are to be subsequently decoded.

An alternative approach is to decode fMRI data based on meta-analyses formed from prior fMRI studies, combining data across different experimental methodologies and parameters (Poldrack, 2006), a process known as reverse inference. This approach has the advantage that it can provide information on a large range of brain functions, which is particularly important when decoding spontaneous events of unknown origin. It has been argued that such reverse inference can have predictive power for a given mental process if a brain region is actively engaged (Poldrack, 2006, Poldrack, 2011), by also taking account of task-setting in which the brain activation occurred as well as existing meta-analysis databases (Hutzler, 2014). However, reverse inference of spontaneous events is particularly challenging since the prior probability of these events is unknown, i.e. decoding is difficult if we have no prior information about what occurred during the data acquisition.

The aim of this study was to decode task-induced and spontaneous events using Sparse Paradigm Free Mapping (SPFM) and meta-analysis. We used SPFM to detect short (3 s) and long (10 s) events in fMRI data without prior information on the timing of any movement or task by using a regularized estimator that deconvolves the fMRI voxel time series assuming a canonical haemodynamic response function (Caballero Gaudes et al., 2013, Petridou et al., 2013). We then derived a decoding score relating detected patterns of motor activity to Activation Likelihood Estimation (ALE) obtained from meta-analysis of task-based fMRI studies (Turkeltaub et al., 2002, Laird et al., 2005). We validated the method by decoding events associated with known responses to a set of six motor movements of short and long duration collected with concurrent electromyography (EMG) recordings. We then used this method to determine the type

of spontaneous movements (within a predefined set of possible movements) undertaken during the period of a resting state fMRI acquisition acquired in the same experimental session.

THEORY

The following section outlines the use of Sparse Paradigm Free Mapping to detect events, and the formation of meta-maps and subsequent decoding of the fMRI data.

(i) Sparse Paradigm Free Mapping (SPFM) for fMRI analysis

Events can be detected within an fMRI dataset using Sparse Paradigm Free Mapping (SPFM), which requires no prior information on their timings. SPFM deconvolves the fMRI signal based on a linear haemodynamic model of the BOLD events using L1-norm regularized regression to give an SPFM activation map for each time frame in the fMRI data series (Caballero Gaudes et al., 2013, Petridou et al., 2013).

(ii) Formation of meta-maps

A meta-map characterizes convergence between the results of different studies and provides a probabilistic atlas of brain function in response to a particular task, which allows us to infer whether activation in a given voxel is likely to be related to a particular task.

Meta-maps can be formed using the Activation Likelihood Estimation (ALE) method implemented in GingerALE Version 2.3 (available at <http://brainmap.org/ale/index.html>) (Eickhoff et al., 2012, Eickhoff et al., 2009, Turkeltaub et al., 2012). The coordinate of brain activation due to a particular task, reported in a particular study considered in the meta-analysis, is known as a 'focus' (Laird et al. 2005). To allow for the uncertainty in the position of the focus due to factors such as inter-subject variability and imperfect anatomical alignment, the probability distribution of the location of the focus is modelled as a 3D Gaussian distribution centered on the focus. Let F_i be the event that any of the foci of activation in response to a particular task from the i^{th} study included in the meta-analysis occurs in the j^{th} voxel, such that $P(F_i)_j$ is the probability that a focus from the i^{th} study occurs in voxel j . If X studies are now considered in the meta-analysis, the probability that a focus from any of the studies occurs in the j^{th} voxel is known as the Activation Likelihood Estimation (ALE) value and is given by the union of all the $P(F_i)_j$, assuming that the results of all the studies are independent (Laird et al., 2005). For example, if there is one focus of activation and the ALE value for the j^{th} voxel is $P(F)_j=0.01$, there is a 1% chance that the focus from any of the studies included in the meta-analysis lay within the j^{th} voxel. A larger ALE value implies that there is a greater chance that one of the foci from the contributing studies lay in that voxel, and so one can infer a higher degree of association between that voxel and the relevant task.

In this study, we defined a meta-map as a map of statistically significant ALE values for a particular task, normalized to allow comparison between different tasks. The number of meta-maps considered, M , determined the number of tasks that could be decoded. Table I shows the $M = 6$ movement task meta-maps considered in this study, together with the total number of voxels with significant ALE values and the range of significant ALE values for each meta-map. Table II shows the overlap between the different meta-map regions. Since the number of studies used to generate each meta-map differed, each meta-map had a different maximum ALE value. This arbitrary difference between ALE values must be overcome in order to use the meta-maps for decoding. Therefore, we normalized each meta-map by the sum of all voxel values within it, to yield a normalized ALE value:

$$\alpha(F)_{j,m} = \frac{P(F)_{j,m}}{\sum_1^J P(F)_{j,m}} \quad [\text{Equation 1}]$$

where J is the total number of voxels in the m -type meta-map and $P(F)_{j,m}$ is the ALE value of voxel j in the m -type meta-map. This normalized ALE value ensured that the probability across a meta-map summed to unity, and could be interpreted as the conditional probability of a focus location being in voxel j given there was a focus in meta-map m .

(iii) Decoding of events

The normalized meta-maps could be used to decode events detected with SPFM at each time frame by estimating a decoding score (D_m) that quantified the spatial overlap between an SPFM activation map and the meta-map associated with the m^{th} movement type, where the abbreviations used to indicate each movement type are indicated in parentheses in Table I. For each fMRI time frame, a non-conservative region of interest (ROI) was defined by applying a low z -threshold to the SPFM activation map. For each of the m meta-maps the normalized ALEs were summed within that ROI to give an Overlap Summation score S_m :

$$S_m(z_T) = \sum_{j=1}^K \alpha(F)_{j,m} \quad [\text{Equation 2}]$$

where K was the total number of voxels in the ROI at a SPFM z -threshold z_T . This process was repeated for sequentially increasing values of z_T within a typical range of SPFM activation z -scores, to obtain values of S_m as a function of SPFM z -threshold. The maximum possible value of S_m would be 1 (Equation 1), which can be interpreted as the probability of a focus from meta-map m being fully contained within the ROI.

The decoding score for each meta-map, D_m , was then defined as the area under the curve of S_m plotted against z_T :

$$D_m = \int_{z_{low}}^{z_{high}} S_m(z_T) dz_T \quad [\text{Equation 3}]$$

where z_{low} and z_{high} were minimum and maximum limits of typical SPFM activation z-scores. A large D_m indicated a large overlap between the SPFM ROI and areas of significantly high ALE value (convergence of foci on the m^{th} meta-map), and thus the SPFM event was likely to involve the task related to that meta-map. Integrating S_m in this way overcame the need to choose a particular threshold, whilst ensuring that a high D_m occurred when the SPFM map overlapped the meta-map across a reasonable range of thresholds. D_m was then converted to a normalized decoding z-score:

$$Z_m = \frac{D_m - \mu_{Dm}}{\sigma_{Dm}} \quad [\text{Equation 4}]$$

where μ_{Dm} and σ_{Dm} were the mean and standard deviation of D_m across all time frames for the m meta-map. False Discovery Rate (FDR) correction was then performed ($q < 0.05$), where the total number of hypotheses was the number of time points multiplied by the number of meta-maps.

This process resulted in M FDR-corrected, time series of decoding z-scores Z_m ($m = 1, \dots, M$). Significant values of Z_m could then be ranked, with the highest rank value of Z_m corresponding to the most likely task type (if any) at each time point.

METHODS

The study was approved by the local Ethics Committee, and all subjects gave informed consent. Nine subjects participated, but datasets from two subjects were discarded due to incomplete data collection. The scan session included (i) short and long motor task fMRI paradigms for validation of the decoding method; (ii) resting state data for spontaneous event decoding assessment.

Paradigm

Motor tasks were used to validate the decoding method due to the high specificity of the Sensorimotor Network (SMN) resulting from the nature of its cortical organization (Penfield and Rasmussen, Penfield and Boldrey, 1937). These tasks involved six motor movements: movement of right or left toes (contraction of all toes of the foot), movement of right or left fingers (thumb brushed against the tips of the rest of the fingers from little finger to first finger with the hand palm facing down), eye blinks and swallowing. Subjects were instructed to perform these movements with minimal head motion.

188

189 Each MR session consisted of two paradigms: RUN1 (resting state and short task scan) and
190 RUN2 (long task scan), chosen to test the algorithm in different conditions and illustrated in
191 Figure 1(a). RUN1 consisted of a 5 minute resting state period followed by 10 minutes in which
192 short motor movements were performed. During the resting state period, a blank screen was
193 displayed and the subjects were instructed to keep their eyes open. Fifteen seconds before the
194 motor movement task paradigm began a “GET READY...” text was displayed on the screen. A
195 simple text instruction was then displayed indicating which movement was to be performed (e.g.
196 “R FOOT”). This was followed by a 3 second countdown display and then a red dot flashed 3
197 times at 1 second intervals. Subjects were instructed to perform each movement task with every
198 flash of the dot, except for the swallowing condition for which one movement was performed
199 within the 3 second interval. A white fixation-cross then appeared for a random inter-stimulus
200 interval of 18-24 seconds before the next movement instruction was displayed. This cycle was
201 repeated twenty-four times (four trials of each movement type) within the 10 minute period.
202 RUN2 consisted of 1 minute when a fixation cross was displayed, followed by 4 minutes of long
203 motor movement tasks and then a further 1 minute of fixation cross. In RUN2 each movement
204 type was performed continuously for a longer 10 second period (red dots flashed 10 times at 1
205 second interval) and swallowing movements were performed twice within the 10 second interval.
206 Only a single repeat was performed for each movement type in RUN2, and the inter-stimulus
207 interval varied randomly between 28-32 seconds.

208

209 Surface electromyography (EMG) was recorded throughout to detect muscle activity during the
210 tasks. MR-compatible electrodes were placed on the arms (on left and right extensor digitorum)
211 and legs (across the lower peroneus longus); these electrodes formed bipolar pairs, which were
212 fed into a MR-compatible bipolar amplifier [ExG amplifier, Brain Products, Munich, Germany], a
213 ground electrode was placed on the right elbow. A MR-compatible unipolar amplifier [MR-plus
214 amplifier, Brain Products, Munich, Germany] was used to measure muscle movement in the neck
215 and head simultaneously. Electrodes were placed above and below the center of the subject's
216 pupil (frontalis and lower orbital orbicularis- right eye only (Blumenthal et al., 2005)), on the jaw
217 (masseter) and the right of neck midline to detect swallowing (approximately on the infrahyoid
218 (Vaiman et al., 2004)), with the reference electrode placed on the nose and the ground electrode
219 on the right mastoid bone. The electrodes were positioned to monitor the movements defined in
220 the meta-maps (see Table I). EMG data were recorded at a sample rate of 5 kHz with a
221 hardware filter set to record in the range 0.016-250 Hz with a roll-off of 30dB/octave at high
222 frequency. All electrodes impedances were kept below 25 k Ω and all electrode leads were
223 twisted to minimize wire loops and the consequential differential effect of the magnetic field on
224 the leads (van Rootselaar et al., 2007). The bipolar amplifier monitoring limb movement was
225 placed at the foot of the scanner bed, whilst the unipolar amplifier monitoring head movements

was placed at the head of the scanner bed. Activity of platysma muscles on the neck could be detected by the electrode on the neck (Vaiman et al., 2004), whilst swallowing movements could be distinguished by their distinctive EMG waveform.

MR Data Acquisition

Data was acquired on a Philips 7 Tesla Achieva scanner [Best, Netherlands] using a 32-channel head coil [Nova Medical]. fMRI data was acquired using axial gradient echo EPI (FOV=208 x 192 x 84 mm, voxel size =2 x 2 x 3 mm³, 28 slices, TE=25 ms, TR=1.5 s, flip angle=64°, SENSE factor 3). To minimize head movements, foam pads were used to constrain the subjects' heads within the head coil. During each fMRI scan, a Vectorcardiogram (VCG) and peripheral pulse unit were used to record the cardiac trace (whichever signal had best quality was used in analysis) and a pneumatic belt placed around the chest was used to record respiratory signals. These signals were collected to allow for physiological noise correction of the fMRI datasets and surface electromyography traces. Following the fMRI data acquisition, a three-dimensional, 1 mm isotropic high resolution T₁-weighted MPRAGE scan and T₂*-weighted spoiled-FLASH scan were acquired.

Data Analysis

EMG data were analyzed using BrainVision Analyzer2 [Brain Products, Munich, Germany]. Gradient and pulse artefact corrections were performed using the average artefact subtraction technique (Allen et al., 2000, Allen et al., 1998). The gradient artefact was corrected on all channels using a sliding window containing 61 volume averages. Pulse artefact correction was performed for the electrodes on the head and neck. The VCG was used to identify the R-peak of the cardiac cycle (Debener et al., 2008, Mullinger et al., 2008, Allen et al., 2000, Allen et al., 1998) and a sliding window of 21 averages was employed in the pulse artefact correction. Absolute differences between active electrode pairs placed on arms, legs, the frontalis and lower orbital orbicularis (for eye movements), and jaw and neck (for swallowing movements) were computed to obtain a single EMG recording to monitor each limb, eye movements and swallowing. The EMG traces were converted to z-scores in MATLAB, and data points with amplitude more than twice the standard deviation of the mean (z-score ≥ 4) were inspected to ensure that they had the appropriate waveform for an EMG trace (to exclude residual gradient artefacts, etc.). The swallowing trace was analyzed by visual inspection since a particular waveform corresponded to swallowing (as opposed to head movement). Markers were manually placed on peaks that reflected both task-related and potential non-task related movements. The final results were visually inspected to discount false positives that could arise from spikes in the traces due to global movements.

Figure 1 (b) summarizes the fMRI data analysis steps. fMRI datasets were realigned [SPM8] (<http://www.fil.ion.ucl.ac.uk/spm/software/spm8/>), physiological noise corrected using RETROICOR (Glover et al., 2000), spatially smoothed with a 4 mm isotropic Gaussian kernel, and low frequency drift corrected up to and including third order fitted polynomials. The effects of signal changes due to sudden head movements were excluded by generating null regressors of those time points with $|d'| > 0.5$ mm/scan where $|d'|$ is the absolute derivative of the net displacement vector from the translational parameters of the realignment procedure (Lemieux et al., 2007).

To increase computational efficiency, each participants' fMRI data was analyzed in four sections: R1 (5 minute rest (resting state), scan dynamics 1-200 of RUN1), M1 (first 5 minutes of short movement task, scan dynamics 201-400 of RUN1), M2 (second 5 minutes of short movement task, scan dynamics 401-642 of RUN1) and M3 (long task, all scan dynamics of RUN2). Voxel-wise mean correction was performed to compute percentage signal change. Voxels with variance in the top 0.5 percentile were excluded from further analysis, since these voxels tend to be related to draining veins. SPfM was performed on the datasets, using the 3dPFM function in MATLAB (now available in AFNI (NIH/NIMH), http://afni.nimh.nih.gov/pub/dist/doc/program_help/3dPFM.html), using L1-norm Dantzig selector regularization path with Bayesian Information Criterion (BIC) for model selection. This produced an Activation Time Series (ATS) indicating time points corresponding to events for every voxel. Realignment parameters along with their Volterra expansion and null regressors (if any) were included as additional covariates (Caballero Gaudes et al., 2013). ATS outputs from SPfM were converted into a time course of maps of Z-scores. The SPfM output was then visually inspected to exclude any time frames that showed strong artefacts at the edges of the brain and brief whole brain activations (assumed to be motion or residual respiratory artefacts not removed by previous procedures).

Creating Meta-maps and Decoding

Meta-maps for each of the six movement types were created from a meta-analysis of 77 fMRI studies of the eye (n=24) mouth (n=18), hand (n=21), and foot (n=14) movements (Table I) using the BrainMap Sleuth Version 2.0 (BrainMap, <http://www.brainmap.org/sleuth/>) (see Supporting Information Tables I-IV). Voxel-wise ALE values were computed for each movement type, and these ALE maps were then thresholded using cluster-level inference correction (Eickhoff et al., 2012). First, a cluster-forming threshold was chosen (uncorrected $p=0.001$). For this threshold, a null distribution of cluster sizes was simulated from 5000 experiments selected at random from the BrainMap database, with the same smoothness as the movement being considered (same number of subjects, and same number of foci). ALE values were computed on the foci from this random set of experiments and the cluster-forming threshold was applied. The resulting cluster

sizes were recorded and the process was repeated to produce a null distribution of cluster sizes. All cluster size values were used in each randomization run. A cluster-level inference threshold of $p=0.01$ was then chosen to determine whether each cluster in the ALE maps was obtained by chance. All ALE computations and cluster level inference correction were performed using GingerALE Version 2.3 software (BrainMap, <http://www.brainmap.org/ale/>) (Eickhoff et al., 2012, Eickhoff et al., 2009, Turkeltaub et al., 2012). The meta-maps were then normalized (see Theory section). The Supplementary Motor Area (SMA) is commonly active in all meta-maps involving sensorimotor tasks, and so to increase functional specificity between the six movement meta-maps, the SMA was masked-out from the ROIs using the SMA mask from the Harvard-Oxford cortical atlas available in FSL (FMRIB, <http://fsl.fmrib.ox.ac.uk/fsl/>).

The decoding z-score Z_m (see Equation 4 in Theory section) was calculated for each meta-map m , at each time point, using trapezoidal numerical integration implemented in MATLAB between SPFM z-threshold limits in steps of $z=0.1$. We chose a non-conservative minimum limit $z_{low}=0.1$ and $z_{high}=6$ since these values were within the typical range of SPFM activation z-scores. Values of $Z_m > 6$ resulted from residual movement artefacts and time frames with such artefact were excluded from analysis. The resulting Z_m timecourses for each movement type m were FDR-corrected ($q=0.05$). Significant decoding z-scores were used to rank the movements in terms of probability of each having occurred at each time point, with the decoded movement type being classified as that with the highest rank.

For task-based paradigms, task stimulus timings and EMG traces were used to validate whether the actual movement took place (task or spontaneous movements). A True Positive (TP) was defined as occurring when the meta-map corresponding to the highest ranked Z_m matched the movement type of the stimulus and was confirmed by the EMG trace. A False Negative (FN) occurred when the decoding method reported the incorrect movement type (FN_{wrong}), or when Z_m failed to decode any event (FN_{null}). **It is not possible to know whether events detected without simultaneous activation in the EMG were actual False Positives since the EMG could only ever record a limited number of movements (restricted by the number of electrodes applied) so we defined these as potential False Positives (Table III).** Decoding sensitivity was calculated as $TP/(TP+ FN)\%$. For resting state data, the decoding z-score of detected spontaneous events was compared in a similar way to potential movements identified in the EMG trace.

RESULTS

EMG data

Upon visual inspection, EMG traces identified task movements cued by visual stimuli during the entire recordings in all subjects, except for Subject 4 and Subject 6. In Subject 4, contact between electrodes with skin surface at the eye, right foot and left foot became loose halfway through the short task experiment, so for those periods the time at which the stimulus cue occurred was used for validation purposes. In Subject 6, no significant EMG spikes were detected for the first left foot movement and second left hand movement, suggesting that this movement was omitted by the subject during the experiment.

Motor Validation Task Data

Figure 2 shows example SPFM maps detected at a time corresponding to a short task movement (visually cued swallowing also detected in EMG - Figure 2 (a)), and with no movement (no task stimulus and no EMG spike detected - Figure 2 (b)). The SPFM activation clusters detected during the swallowing task overlapped areas of significant Activation Likelihood Estimation (ALE) values for mouth movements in the corresponding meta-map. During the period of no movement, no activation was detected in the mouth movement meta-map ROIs (or indeed other motor ROIs), although a small area of activation can be seen posterior to the motor areas. Figures 2 (c) and 2 (d) plot the corresponding Overlap Summation score S_m (Equation 2) for the 6 movement meta-maps and also list the decoding scores D_m , based on the area under each of the curves (Equation 3). For short movement task, large activated regions with high z-scores were detected by SPFM, resulting in high S_m values that persisted at higher SPFM z-threshold, particularly when there was large overlap between the activation map and meta-map. In contrast, for the period of no movement the values of the overlap summation S_m were small at low SPFM z-threshold and decreased rapidly with higher SPFM z-threshold for all movement types, since less activation was detected by SPFM.

Figure 3 shows the time course of the decoding z-score Z_m for each meta-map and the corresponding EMG z-score traces for the short motor tasks for Subject 1. Task-induced motor movements were detected by EMG at the time of the visually-cued stimuli (indicated by dotted red lines). Other spikes were detected sporadically in the EMG traces due to spontaneous (non-task) movements or possible residual movements related to tasks due to close proximity of leads leading to the EMG breakout box. Swallowing events are not as apparent in the EMG traces as other movements, but they were detected by their distinctive waveforms, rather than by peaks in the EMG amplitude. Peaks in the appropriate decoding z-score timecourse were generally observed at the time of the visually cued stimulus for hand (LH and RH), foot (LF and RF) and mouth (Mo) movements. For eye blinks (E), the decoding score Z_E failed to detect any task-based movements. Two non-task-based swallowing movements were detected in the EMG traces during the left foot and left hand motor tasks at scan dynamics 110 and 137 respectively (green crosses). At these time points Z_{LF} and Z_{LH} had higher amplitudes than Z_{Mo} . Figure 4

compares all decoding score with all tasks for all subjects. It can be seen that, excluding eye movements, the highest ranked decoding score correspond to the correct (task) movement type. Peaks in the decoding z-score were also found that were neither task-related nor associated with EMG, for example at time points 184 (LF), 240 (M) and 390 (M) for Subject 1.

Table IV summarizes the validation results from all subjects for RUN 1 (short motor task). This table shows that generally events were successfully decoded for hand, foot and mouth movements across all subjects. Table IV (a) indicates how often the maximum meta-map decoding score corresponded to a correct movement type. The average successful decoding rate was $66 \pm 7\%$ averaging across all subjects and movement types ($77 \pm 13\%$ when eye movements were excluded). The decoding rate was only $11 \pm 18\%$ for eye movements across all subjects, for which all false negatives were due to no event being decoded (FN_{null}) (no significant overlap between meta-map and activation). From Table IV (b), it is also apparent that, besides Subject 3, most of False Negatives were FN_{null} , but hand movements had a higher misclassification rate (FN_{wrong} greater than FN_{null}). Importantly for Subject 6, no significant EMG spikes were detected for the first left foot movement and second left hand movement, suggesting that this movement was not performed, the decoding results supported this finding since no foot movement was decoded at these time points. Table IV (e) also shows the number of null regressors included and suggests a relationship between decoding accuracy and lack of movement artefacts. Spontaneous (non-tasked) movements were also detected by EMG (trace not shown in Figure 4), and some of these were successfully decoded for Subject 3 (24%) and Subject 4 (8%), Table V. There were also a number of decoded events that were not associated to any stimuli or EMG traces (excluding eye movements), shown in Table IV (d), which could be interpreted as false positives for the decoding but may be related to activity not detected by EMG. **It is not possible to calculate Positive Predicted Value $[TP/(TP + FP)]$ since we cannot confidently label detected events not associated with task or EMG as false positives (FP), since the EMG is unable to detect all possible movements. However, assuming that all potential false positives are actual false positives, the minimum Positive Predicted value would be 77% (range 64-100%).**

Figure 5 and Table VI summarize the results for RUN2 (long motor task). For Subject 1, at time point 41 there was an increase in decoding score for all movement types, indicating possible head movement that was not excluded by the null regressors (the absolute derivative of the net displacement vector of translational head motion at that time point was $|d'|=0.41$ mm/scan). The average successful decoding rate for the long task was $74 \pm 16\%$ excluding eye movements. In contrast to the short movement task, most False Negatives in the long movement task were attributed to misclassification (FN_{wrong}). **The minimum Positive Predicted value would be 47% (range 30-83%).**

For the resting state dataset, SPFM detected spontaneous events in the Sensorimotor Network (SMN) that were not attributed to any given task. Asterisks indicate events that were found by decoding and confirmed by EMG. Figure 6 illustrates the variation in the types and durations of movement detected on EMG and decoded events between subjects in the resting state. The meta-maps overlaid on the SPFM maps for corresponding decoded events, corresponding to particular movements detected by EMG at rest for Subject 1 are also shown at the top of Figure 6. Table VII (a) shows the fraction of spontaneous events for which the decoding agreed with the movement simultaneously detected on EMG. Table VII (b) summarizes spontaneous events that were detected at rest with significant decoding score, but which were not associated with any event detected by EMG.

DISCUSSION

We have demonstrated a method for decoding movement events in fMRI data with no prior knowledge of the nature of the movement and without using training data sets. Instead, we used Activation Likelihood Estimation and coordinate based meta-analysis. The decoding ranks the potential decoded movements at each time point, with the highest rank taken as the most probable movement type. We have validated the method on both long and short movement tasks, and have also shown that it can decode spontaneous activity occurring in resting state data.

There has been substantial development in fMRI brain decoding in recent years involving visual perception, visual features, visual objects, novel visual scenes, attention processes, imagery and working memory, episodic memory, semantic knowledge and phonological representations (Tong and Pratte, 2012). Most of these methods use machine learning algorithms such as Support Vector Machines (SVM) to train a classifier to recognize spatial patterns in order to decode. Several studies have applied machine learning algorithms to decode non-task brain activity by building a classifier based on tasks. Schrouff et al. utilized machine learning (Gaussian Processes classifier) trained on three mental imagery tasks to access activity during rest periods before and after tasks (Schrouff et al., 2012a, Schrouff et al., 2012b). Although the results suggested that classification of resting state sessions can be performed by applying previously trained classifiers, this method is limited to the number of categories the decoder is trained for. Although our method is also limited to the number of meta-maps considered, it is easier to extend it by generating meta-maps for more categories from a large database of literature, compared to reconstructing new experiments to train the decoder. The concept of decoding using meta-analysis is supported by the availability of large-scale automated meta-analysis of fMRI data. *Neurosynth* (NIH, <http://neurosynth.org/>) (Yarkoni et al., 2011) measures similarity between a spatial activation map (such as T-map obtained using General Linear Models

analysis) and patterns associated with 'cognitive maps' available in its database using a spatial correlation (Pearson correlation). To our best knowledge, no method has been developed to decode spontaneous events quantitatively by means of voxel-wise coordinate-based meta-analysis measures and without prior experiments undertaken by the subject being investigated.

Depending on computational resources available, the method described is potentially time consuming to implement and run, but has the potential to provide unique information about behavior in the resting state, and separating of distinct behaviors from other brain activity. This could be useful in many ways, for instance, in clinical research studying somatic pain in conditions such as irritable bowel syndrome, or in psychological research in naturalistic paradigms or into emotional congruence.

Validation

We validated the technique using task-based data where the movement was confirmed by EMG. The decoding method was validated against 24 short task movement trials (3 seconds duration with 1 movement performed per second for each trial), and also against spontaneous events (which are inevitably quite sparse). We found good agreement between decoding results and EMG for most events and subjects, with a range in sensitivity between 55 and 100% excluding eye movements. The sensitivity was lowest for Subject 3, probably related to the fact that this subject showed more motion. Across all subjects, only 11% of short eye movement tasks were successfully detected (high FN_{null}), probably because of the smaller BOLD signal in response to eye movements, which may be because eye blinks are very common movements that involve a smaller muscle volume compared to many other movements. Furthermore, there is a lack of fMRI literature on eye blinks, so that the studies included in the eye movement meta-map were predominantly eye saccades, which will not have been ideal for decoding eye blinks. This illustrates that decoding can only be achieved reliably if appropriate metamaps are available.

During any tasked movement, the decoding score was largest for the meta-map corresponding to the movement being undertaken, but also tended to increase for other movement types. This may be due to overlap between the meta-maps (shown in Table II) or because activation was not confined to the region of a single meta-map during a particular movement. This could indicate a lack of selectivity in the brain's response to a particular behavior, or functional connectivity within the SMN that is activated as a whole during a given movement (Biswal et al., 1995), although the SMA was masked out during the analysis to increase specificity to different motor activations. Alternatively, it could be due to imperfect registration of meta-maps to the subject's data space or subject anatomical variability.

Events may not have been decoded successfully, either because no activation was detected by SPFM or because the activation did not adequately overlap the appropriate meta-map. One

problem with the validation was that although we detected unexplained events (peaks in the decoding traces that were not detected by EMG - potential false positives), it was impossible to determine if these were actual false positives and hence specificity. Some such peaks are always expected since the EMG electrodes were placed at specific muscle locations, and thus not sensitive to all types of movements included in the meta-analysis; the proposed decoding method might provide the only means of interpreting such spontaneous activations. Nonetheless for Subject 6 where no EMG events were detected corresponding to tasked short movements, the method also decoded no movements, strongly suggesting that no movement was actually performed by the subject. The EMG setup was carefully designed to minimize artefacts due to the MRI environment, in particular limiting movement of the electrode leads when the subjects performed a movement. Nonetheless, visual inspection of the thresholded EMG traces showed that some residual lead movements were still picked up by nearby EMG channels (Figure 3). Further validation work would be simplified if movements could be automatically detected in the EMG trace, either by detecting non-periodic perturbations in the traces, or by pattern recognition of waveform patterns in a sliding window approach.

Spontaneous events

Although the term “resting state” is usually interpreted as no task being undertaken, in reality the brain is always actively performing tasks involving internal or external thoughts, or movements (Binder et al., 1999). Here we confirmed our previous finding that some spontaneous events in the Sensorimotor Network are in fact spontaneous movements as detected by EMG (Petridou et al., 2013). We have previously suggested that functional connectivity is somewhat driven by such spontaneous BOLD events (Allan et al., 2015, Petridou et al., 2013). To what extent these spontaneous events may cause differences in connectivity due to inter-subject or inter-group behavior variability is of great interest but still unknown.

Non-tasked movements that occur at rest are often shorter and smaller than task-induced movements, generally causing weaker fMRI activations of smaller spatial extent, and thus insignificant decoding scores. Similarly non-tasked movements also produce lower EMG scores particularly since the EMG was probably not set up to detect the exact spontaneous movement being undertaken. **These reasons will have led to, spontaneous events being less likely to be detected, decoded, and confirmed by EMG.** However, we expect that faster sampling of fMRI data, for instance using simultaneous multi-slice imaging (Feinberg et al., 2010, Moeller et al., 2010), will provide significantly increased sensitivity to improve decoding. **Furthermore, the underlying SPFM algorithms are designed to enforce sparsity in the number of events, but this might be relaxed particularly since the final statistical test for the decoding is much more stringent since it is based on the pattern of activation rather than a single voxel time course.** Some spontaneous events were detected in resting state data with significant decoding score, but were not associated with any event detected by EMG. At this stage it is impossible to

know whether these events relate to spontaneous movements, reflect such lack of sensitivity in EMG, or reflect some other underlying spontaneous activity in the SMN, such as motor imagery or planning of action (Mizuguchi et al., 2014).

In principle, this approach could be extended to study non-motor brain functions by including metamaps for a wider range of tasks, but this will pose a number of challenges. Firstly, the signals are sometimes smaller in the non-motor networks making detection and decoding more difficult. Secondly, the validation will be more complicated if there is no overt response involved, this might be addressed controlling the state of a subject (e.g. in naturalistic paradigms such as watching a movie) (Hasson et al.).

Methodology

This section discusses the methodology implications and improvements that can be made to increase the decoding performance in more detail. The TR was 1.5s, limiting the temporal resolution of the data set. Therefore, the 3 events occurring in the short paradigm or the 10 events occurring in the long paradigm could not be separated, although the individual events were apparent in the EMG trace. Despite the temporal blurring of the hemodynamic response, we predict that increased temporal resolution, for instance by using simultaneous multi-slice imaging (Feinberg et al., 2010; Moeller et al., 2010), would help to differentiate between individual movements within blocks, in addition to enhancing the performance of the SPFM deconvolution, and consequently the decoding accuracy. This can be pursued in future as fast fMRI sequences become more routinely available.

The proposed technique depends on the success of SPFM in detecting events. The combination of the L1-norm (sparse regression) and Bayesian Information Criteria model selection in SPFM controls the number of false positives for event detection (Caballero Gaudes et al., 2013). However, fMRI datasets that are corrupted by large motion artefacts and physiological noise may still have residual noise even after standard motion and physiological noise corrections. In this study, we included six translational motion regressors with their Volterra expansion as regressors for SPFM (Lemieux et al., 2007), and omitted voxels that displayed high variance which were probably due to draining vein artefacts. We also excluded frames by using null regressors where the displacement vector was greater than 0.5 mm per scan and visually scrutinized the SPFM results to exclude time frames that were suspected of containing other artefacts. Alternatively, other methods based on ICA decomposition and the identification of artefactual independent components, such as FIX (Griffanti et al., 2014, Salimi-Khorshidi et al., 2014) or AROMA (Pruim et al., 2015a, Pruim et al., 2015b), or more sophisticated tissue-based nuisance regression such as ANATICOR (Jo et al., 2010, Jo et al., 2013) could be explored to further reduce artefacts and physiological noise from the fMRI data. For the long task (RUN 2), the decoded activations did not extend through the entire stimulus duration (Figure 5). In future work, more sophisticated

SPFM algorithms using a structured L1-norm regularization, such as Fused Lasso or Smooth Lasso (Caballero-Gaudes et al., 2012, Hernandez-Garcia and Ulfarsson, 2011) could provide a more accurate deconvolution for prolonged and intermixed stimuli than the Dantzig Selector, potentially improving decoding accuracy.

The method also depends on the accuracy of meta-maps, how well they correspond to the tasks being undertaken, and the overlap between them. The failure to decode eye movements in this study highlights that it is essential for studies used in the meta-analysis to be as similar as possible to the movement type to be decoded. The proposed decoding methodology required maps of expected patterns of activation in response to particular behaviors and for this it uses meta-analysis of many fMRI studies, rather than subject-specific data, although ALE attempts to account for intersubject variance by modelling the location of the activation as a Gaussian distribution. Using datasets acquired from the subject under investigation would increase the sensitivity by providing better overlap between the SPFM and meta-maps matching the subject's anatomy. This might particularly benefit the decoding of more subtle activations seen in the resting state. However, this would greatly reduce the usefulness of the technique, as it would require all activations of interest to be mapped prior to the decoding experiment for each subject, rather than building on the expanse of fMRI literature. Increasing the number of studies used in the meta-analysis might also increase the accuracy of ALEs. An alternative approach is to integrate SPFM results with *Neurosynth* (NIH, <http://neurosynth.org/>), a platform that synthesizes activation results from many different fMRI studies (Yarkoni et al., 2011).

Meta-analysis works well in Sensorimotor Network due to the high selectivity of its cortical organization with limited overlap between activated regions for different motor tasks (Penfield and Rasmussen, Penfield and Boldrey, 1937, Schott, 1993). Here we developed a method of increasing selectivity by masking out the SMA region common to all movement tasks, and further masks could be applied to focus on smaller activated areas (e.g. to decode which finger was being moved (Sanchez-Panchuelo et al.)). Conversely, if the aim were to separate primary types of activation (e.g. visual and motor), then the mask over the SMA could be removed. Extending the decoding method to cognitive resting state networks may be challenging since there is less functional selectivity in the relevant activation maps, which might thus reduce the likelihood of a valid reverse inference (Hutzler, 2014, Poldrack, 2011).

In developing this method, we explored several alternative methods of estimating the probability that an activation area was related to a task. Simple binary conjunction between activation maps and meta-maps did not take into account the difference in z-score magnitudes of the SPFM and ALE values. Similarly, spatial correlation between activation and meta-maps was not appropriate since meta-maps are built from Gaussian distributions around foci of activations, which do not take account of the underlying shape of the pattern of activation in the individual studies, which are reflected in SPFM maps. Multiplying activation maps (z-scores) and meta-maps (via p-values

converted to z-scores) together can produce a high product value either due to the activation, the ALE or both, and these situations cannot be distinguished. Building a multivariate distribution from both the ALE z-scores and SPFM z-distribution was not appropriate because the joint distribution was generally biased along the axis of the SPFM distribution, making it impossible to define a simple confidence interval ellipse to detect outliers.

The 'decoding z-score' developed here is a measure of overlap of SPFM spatial activations with the ALE meta-maps. An advantage of this approach is that it does not require a fixed threshold to be applied to SPFM z-scores, which is important since SPFM z-scores can vary significantly between scans, depending on fMRI data quality and inter-subject differences in BOLD response amplitude. The meta-maps were normalized to allow fair comparison between them. This normalization process assumes that behaviors corresponding to each of the M meta-maps are equally likely to occur in any given time frame. This is reasonable since each time frame is analyzed independently, which is fundamental to the concept of detecting and decoding spontaneous events. If the prior probability of certain events were known for some circumstances, the proposed **method could be adapted to consider this information.**

The decoding performance reported here is lower than that reported for decoding methods based on machine learning or Multivoxel Pattern Analysis (MVPA). However, to our knowledge, previous attempts at decoding based on MVPA have been constrained by the need to acquire training data at an individual level. The proposed method decodes data from one individual using a meta-analysis of fMRI data, i.e. acquired on other individuals and at other times and locations, trading decoding power for lifting the constraint of needing to acquired training data. Future work should investigate whether the combination of machine learning approaches with fMRI meta-analyses would give increased decoding power, although the overlap measures used here could still be used as a measure of the contribution of different behaviors to a particular event.

CONCLUSION

To conclude, this work provides a novel method to decode events detected in fMRI data using Sparse Paradigm Free Mapping in combination with brain decoding based on meta-analysis. After validation in tasked motor movements, the proposed method has determined the nature of spontaneous movements undertaken in the apparent resting state, and we have confirmed these finding using EMG. These results underline our assertion that functional connectivity analysis of resting state data is inevitably affected by spontaneous and unpredictable behaviors. The decoding technique proposed here provides a means of interpreting such spontaneous activity. It is now necessary to determine the sensitivity of these methods to more subtle behaviors and responses.

634

635

636 REFERENCES

- 637 ALLAN, T. W., FRANCIS, S. T., CABALLERO-GAUDES, C., MORRIS, P. G., LIDDLE, E. B., LIDDLE,
638 P. F., BROOKES, M. J. & GOWLAND, P. A. 2015. Functional Connectivity in MRI Is
639 Driven by Spontaneous BOLD Events. *PLoS ONE*, 10, e0124577.
- 640 ALLEN, P. J., JOSEPHS, O. & TURNER, R. 2000. A method for removing imaging artifact from
641 continuous EEG recorded during functional MRI. *Neuroimage*, 12, 230-9.
- 642 ALLEN, P. J., POLIZZI, G., KRAKOW, K., FISH, D. R. & LEMIEUX, L. 1998. Identification of EEG
643 events in the MR scanner: the problem of pulse artifact and a method for its
644 subtraction. *Neuroimage*, 8, 229-39.
- 645 BINDER, J. R., FROST, J. A., HAMMEKE, T. A., BELLGOWAN, P. S., RAO, S. M. & COX, R. W.
646 1999. Conceptual processing during the conscious resting state. A functional MRI
647 study. *J Cogn Neurosci*, 11, 80-95.
- 648 BISWAL, B., YETKIN, F. Z., HAUGHTON, V. M. & HYDE, J. S. 1995. Functional connectivity in
649 the motor cortex of resting human brain using echo-planar MRI. *Magn Reson Med*,
650 34, 537-41.
- 651 BLUMENTHAL, T. D., CUTHBERT, B. N., FILION, D. L., HACKLEY, S., LIPP, O. V. & VAN BOXTEL,
652 A. 2005. Committee report: Guidelines for human startle eyeblink electromyographic
653 studies. *Psychophysiology*, 42, 1-15.
- 654 CABALLERO-GAUDES, C., KARAHANOGU, F. I., LAZEYRAS, F. & VAN DE VILLE, D. Structured
655 sparse deconvolution for paradigm free mapping of functional MRI data. Biomedical
656 Imaging (ISBI), 2012 9th IEEE International Symposium on, 2-5 May 2012 2012. 322-
657 325.
- 658 CABALLERO GAUDES, C., PETRIDOU, N., FRANCIS, S. T., DRYDEN, I. L. & GOWLAND, P. A.
659 2013. Paradigm free mapping with sparse regression automatically detects single-
660 trial functional magnetic resonance imaging blood oxygenation level dependent
661 responses. *Human brain mapping*, 34, 501-18.
- 662 CHEN, J. E., CHANG, C., GREICIUS, M. D. & GLOVER, G. H. 2015. Introducing co-activation
663 pattern metrics to quantify spontaneous brain network dynamics. *Neuroimage*, 111,
664 476-88.
- 665 CISLER, J. M., BUSH, K. & STEELE, J. S. 2014. A comparison of statistical methods for
666 detecting context-modulated functional connectivity in fMRI. *Neuroimage*, 84, 1042-
667 52.
- 668 COX, D. D. & SAVOY, R. L. 2003. Functional magnetic resonance imaging (fMRI) "brain
669 reading": detecting and classifying distributed patterns of fMRI activity in human
670 visual cortex. *Neuroimage*, 19, 261-70.
- 671 DEBENER, S., MULLINGER, K. J., NIAZY, R. K. & BOWTELL, R. W. 2008. Properties of the
672 ballistocardiogram artefact as revealed by EEG recordings at 1.5, 3 and 7 T static
673 magnetic field strength. *Int J Psychophysiol*, 67, 189-99.
- 674 EICKHOFF, S. B., BZDOK, D., LAIRD, A. R., KURTH, F. & FOX, P. T. 2012. Activation likelihood
675 estimation meta-analysis revisited. *Neuroimage*, 59, 2349-61.
- 676 EICKHOFF, S. B., LAIRD, A. R., GREFKES, C., WANG, L. E., ZILLES, K. & FOX, P. T. 2009.
677 Coordinate-based activation likelihood estimation meta-analysis of neuroimaging
678 data: a random-effects approach based on empirical estimates of spatial uncertainty.
679 *Hum Brain Mapp*, 30, 2907-26.

- FEINBERG, D. A., MOELLER, S., SMITH, S. M., AUERBACH, E., RAMANNA, S., GLASSER, M. F., MILLER, K. L., UGURBIL, K. & YACOUB, E. 2010. Multiplexed Echo Planar Imaging for Sub-Second Whole Brain fMRI and Fast Diffusion Imaging. *PLoS ONE*, 5, e15710.
- GAUDES, C. C., PETRIDOU, N., DRYDEN, I. L., BAI, L., FRANCIS, S. T. & GOWLAND, P. A. 2011. Detection and characterization of single-trial fMRI bold responses: paradigm free mapping. *Human brain mapping*, 32, 1400-18.
- GLOVER, G. H., LI, T. Q. & RESS, D. 2000. Image-based method for retrospective correction of physiological motion effects in fMRI: RETROICOR. *Magn Reson Med*, 44, 162-7.
- GRIFFANTI, L., SALIMI-KHORSHIDI, G., BECKMANN, C. F., AUERBACH, E. J., DOUAUD, G., SEXTON, C. E., ZSOLDOS, E., EBMEIER, K. P., FILIPPINI, N., MACKAY, C. E., MOELLER, S., XU, J., YACOUB, E., BASELLI, G., UGURBIL, K., MILLER, K. L. & SMITH, S. M. 2014. ICA-based artefact removal and accelerated fMRI acquisition for improved resting state network imaging. *Neuroimage*, 95, 232-47.
- HASSON, U., FURMAN O FAU - CLARK, D., CLARK D FAU - DUDAI, Y., DUDAI Y FAU - DAVACHI, L. & DAVACHI, L. Enhanced intersubject correlations during movie viewing correlate with successful episodic encoding.
- HAXBY, J. V., GOBBINI, M. I., FUREY, M. L., ISHAI, A., SCHOUTEN, J. L. & PIETRINI, P. 2001. Distributed and overlapping representations of faces and objects in ventral temporal cortex. *Science*, 293, 2425-30.
- HAYNES, J. D. & REES, G. 2005. Predicting the stream of consciousness from activity in human visual cortex. *Curr Biol*, 15, 1301-7.
- HERNANDEZ-GARCIA, L. & ULFARSSON, M. O. 2011. Neuronal event detection in fMRI time series using iterative deconvolution techniques. *Magn Reson Imaging*, 29, 353-64.
- HORIKAWA, T., TAMAKI, M., MIYAWAKI, Y. & KAMITANI, Y. 2013. Neural decoding of visual imagery during sleep. *Science*, 340, 639-42.
- HUTZLER, F. 2014. Reverse inference is not a fallacy per se: Cognitive processes can be inferred from functional imaging data. *NeuroImage*, 84, 1061-1069.
- JO, H. J., GOTTS, S. J., REYNOLDS, R. C., BANDETTINI, P. A., MARTIN, A., COX, R. W. & SAAD, Z. S. 2013. Effective Preprocessing Procedures Virtually Eliminate Distance-Dependent Motion Artifacts in Resting State FMRI. *J Appl Math*, 2013.
- JO, H. J., SAAD, Z. S., SIMMONS, W. K., MILBURY, L. A. & COX, R. W. 2010. Mapping sources of correlation in resting state FMRI, with artifact detection and removal. *Neuroimage*, 52, 571-82.
- KAMITANI, Y. & TONG, F. 2005. Decoding the visual and subjective contents of the human brain. *Nat Neurosci*, 8, 679-85.
- KARAHANOGU, F. I., CABALLERO-GAUDES, C., LAZEYRAS, F. & VAN DE VILLE, D. 2013. Total activation: fMRI deconvolution through spatio-temporal regularization. *Neuroimage*, 73, 121-34.
- LAIRD, A. R., FOX, P. M., PRICE, C. J., GLAHN, D. C., UECKER, A. M., LANCASTER, J. L., TURKELTAUB, P. E., KOCHUNOV, P. & FOX, P. T. 2005. ALE meta-analysis: Controlling the false discovery rate and performing statistical contrasts. *Human brain mapping*, 25, 155-164.
- LEMIEUX, L., SALEK-HADDADI, A., LUND, T. E., LAUFS, H. & CARMICHAEL, D. 2007. Modelling large motion events in fMRI studies of patients with epilepsy. *Magn Reson Imaging*, 25, 894-901.
- LIU, X., CHANG, C. & DUYN, J. H. 2013. Decomposition of Spontaneous Brain Activity into Distinct fMRI Co-activation Patterns. *Frontiers in Systems Neuroscience*, 7.

- MIZUGUCHI, N., NAKATA, H. & KANOSUE, K. 2014. Effector-independent brain activity during motor imagery of the upper and lower limbs: An fMRI study. *Neuroscience Letters*, 581, 69-74.
- MOELLER, S., YACOB, E., OLMAN, C. A., AUERBACH, E., STRUPP, J., HAREL, N. & UGURBIL, K. 2010. Multiband multislice GE-EPI at 7 tesla, with 16-fold acceleration using partial parallel imaging with application to high spatial and temporal whole-brain fMRI. *Magn Reson Med*, 63, 1144-53.
- MULLINGER, K. J., MORGAN, P. S. & BOWTELL, R. W. 2008. Improved artifact correction for combined electroencephalography/functional MRI by means of synchronization and use of vectorcardiogram recordings. *J Magn Reson Imaging*, 27, 607-16.
- O'CRAVEN, K. M. & KANWISHER, N. 2000. Mental Imagery of Faces and Places Activates Corresponding Stimulus-Specific Brain Regions. *J. Cognitive Neuroscience*, 12, 1013-1023.
- O'TOOLE, A. J., JIANG, F., ABDI, H. & HAXBY, J. V. 2005. Partially distributed representations of objects and faces in ventral temporal cortex. *J Cogn Neurosci*, 17, 580-90.
- PENFIELD, W. & BOLDREY, E. 1937. SOMATIC MOTOR AND SENSORY REPRESENTATION IN THE CEREBRAL CORTEX OF MAN AS STUDIED BY ELECTRICAL STIMULATION. *Brain*, 60, 389-443.
- PENFIELD, W. & RASMUSSEN, T. *The Cerebral Cortex of Man*.
- PETRIDOU, N., GAUDES, C. C., DRYDEN, I. L., FRANCIS, S. T. & GOWLAND, P. A. 2013. Periods of rest in fMRI contain individual spontaneous events which are related to slowly fluctuating spontaneous activity. *Human brain mapping*, 34, 1319-1329.
- POLDRACK, R. A. 2006. Can cognitive processes be inferred from neuroimaging data? *Trends in Cognitive Sciences*, 10, 59-63.
- POLDRACK, RUSSELL A. 2011. Inferring Mental States from Neuroimaging Data: From Reverse Inference to Large-Scale Decoding. *Neuron*, 72, 692-697.
- PRUIM, R. H., MENNES, M., BUITELAAR, J. K. & BECKMANN, C. F. 2015a. Evaluation of ICA-AROMA and alternative strategies for motion artifact removal in resting state fMRI. *Neuroimage*, 112, 278-87.
- PRUIM, R. H., MENNES, M., VAN ROOIJ, D., LLERA, A., BUITELAAR, J. K. & BECKMANN, C. F. 2015b. ICA-AROMA: A robust ICA-based strategy for removing motion artifacts from fMRI data. *Neuroimage*, 112, 267-77.
- SALIMI-KHORSHIDI, G., DOUAUD, G., BECKMANN, C. F., GLASSER, M. F., GRIFFANTI, L. & SMITH, S. M. 2014. Automatic denoising of functional MRI data: combining independent component analysis and hierarchical fusion of classifiers. *Neuroimage*, 90, 449-68.
- SANCHEZ-PANCHUELO, R. M., FRANCIS S FAU - BOWTELL, R., BOWTELL R FAU - SCHLUPPECK, D. & SCHLUPPECK, D. Mapping human somatosensory cortex in individual subjects with 7T functional MRI.
- SCHOTT, G. D. 1993. Penfield's homunculus: a note on cerebral cartography. *Journal of Neurology, Neurosurgery, and Psychiatry*, 56, 329-333.
- SCHROUFF, J., KUSSE, C., WEHENKEL, L., MAQUET, P. & PHILLIPS, C. Decoding Spontaneous Brain Activity from fMRI Using Gaussian Processes: Tracking Brain Reactivation. Pattern Recognition in NeuroImaging (PRNI), 2012 International Workshop on, 2-4 July 2012 2012a. 61-64.

- SCHROUFF, J., KUSSE, C., WEHENKEL, L., MAQUET, P. & PHILLIPS, C. 2012b. Decoding Semi-Constrained Brain Activity from fMRI Using Support Vector Machines and Gaussian Processes. *PLoS ONE*, 7, e35860.
- SMITH, S. M., MILLER, K. L., MOELLER, S., XU, J., AUERBACH, E. J., WOOLRICH, M. W., BECKMANN, C. F., JENKINSON, M., ANDERSSON, J., GLASSER, M. F., VAN ESSEN, D. C., FEINBERG, D. A., YACOB, E. S. & UGURBIL, K. 2012. Temporally-independent functional modes of spontaneous brain activity. *Proc Natl Acad Sci U S A*, 109, 3131-6.
- TONG, F. & PRATTE, M. S. 2012. Decoding Patterns of Human Brain Activity. *Annual Review of Psychology*, Vol 63, 63, 483-509.
- TURKELTAUB, P. E., EDEN, G. F., JONES, K. M. & ZEFFIRO, T. A. 2002. Meta-analysis of the functional neuroanatomy of single-word reading: Method and validation. *NeuroImage*, 16, 765-780.
- TURKELTAUB, P. E., EICKHOFF, S. B., LAIRD, A. R., FOX, M., WIENER, M. & FOX, P. 2012. Minimizing within-experiment and within-group effects in Activation Likelihood Estimation meta-analyses. *Hum Brain Mapp*, 33, 1-13.
- VAIMAN, M., EVIATAR, E. & SEGAL, S. 2004. Surface electromyographic studies of swallowing in normal subjects: a review of 440 adults. Report 3. Qualitative data. *Otolaryngology--head and neck surgery : official journal of American Academy of Otolaryngology-Head and Neck Surgery*, 131, 977-85.
- VAN ROOTSELAAR, A.-F., RENKEN, R., DE JONG, B. M., HOOGDUIJN, J. M., TIJSEN, M. A. J. & MAURITS, N. M. 2007. fMRI analysis for motor paradigms using EMG-based designs: A validation study. *Human brain mapping*, 28, 1117-1127.
- YARKONI, T., POLDRACK, R. A., NICHOLS, T. E., VAN ESSEN, D. C. & WAGER, T. D. 2011. Large-scale automated synthesis of human functional neuroimaging data. *Nature Methods*, 8, 665-U95.

FIGURE LEGEND

Figure 1 (a): Experiment paradigm of RUN1 and RUN2. RUN1 comprised a 5 minute rest period followed by 10 minutes of short motor movement task (twenty-four 3-second motor task trials performed separated by a random inter-stimulus interval (ISI) of 18-24 seconds). 3 movements were done in each short task trial, with four trial repetitions of each movement type except for the swallowing movement which was performed once. RUN2 comprised a 1 minute green fixation cross, followed by a 4 minute long motor movement task (six 10-second motor task trials with random ISI of 28-32 seconds), and then a further 1 minute of fixation cross. 10 movements were done in each long task trial, except for swallowing movement which were performed twice, with one trial repetition of each movement type. (b): Flow chart of decoding method. SPFM was performed on pre-processed data from RUN1 and RUN2. Six meta-maps were generated for each movement type using cluster-level inference in GingerALE. A decoding z-score, Z_m was then computed for each meta-map m at each time point to quantify spatial overlap between SPFM activation time frames and the m^{th} meta-map. All decoding scores were FDR-corrected ($q < 0.05$).

Figure 2: (a) Example SPFM map (red-yellow) for Subject 1 produced at time frame 154 of the short task RUN1 during a swallowing condition of the movement task detected by EMG. The SPFM map is overlaid on the corresponding meta-map (green). (b) SPFM map (red-yellow) produced at time frame 10 of the short task RUN1 (no movement expected or detected by EMG) overlaid on corresponding meta-map (green). (c) Overlap Summation score S_m for all movement types for time frame 154. (d) Overlap Summation score S_m for all movement types for time frame 10. The decoding score, D_m , which is the area under each curves for (c) and (d), is given in respective colors indicated in the legend.

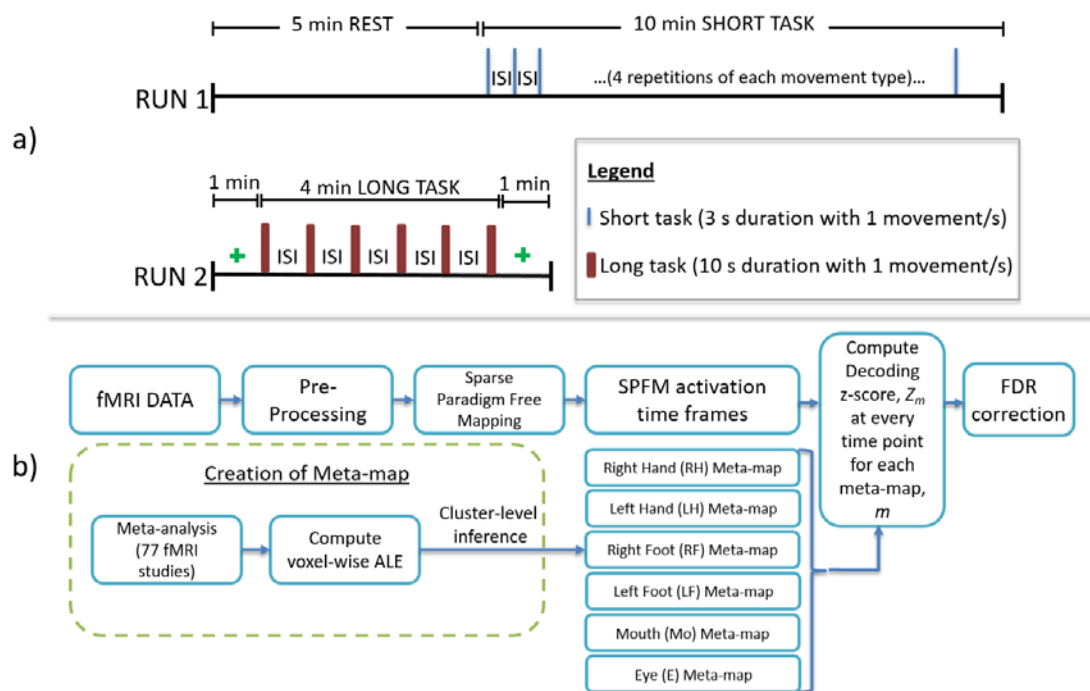
Figure 3: Decoding z-score Z_m (top row) and EMG z-score trace (bottom row) during short task paradigm in Subject 1 for each movement type: eye (E), swallowing (Mo), left hand (LH), right hand (RH), left foot (LF) and right foot (RF). Vertical dotted red lines indicate the times of the visual-cue stimulus, and vertical dotted green lines indicate movement detected by EMG trace. Horizontal aqua lines in EMG traces indicate $|z| > 4$. Spikes in mouth EMG traces are not as apparent compared to other EMG traces because swallowing movements are reflected as distinctive waveform patterns, rather than an amplitude of the signal. Two non-task-based swallowing movement were detected by the decoding z-score at scan dynamic 110 and 137 (indicated by green cross), however Z_{LF} and Z_{LH} at these time points had higher magnitude than Z_{Mo} .

Figure 4: Decoding z-scores (FDR corrected, $q=0.05$) during short task for all subjects. The colored bands indicate the tasked stimulus given to the subject. The colored lines show the decoding z-scores for each meta-map type. The movement type with the highest decoding z-score is indicated by a colored square. The decoded movement types generally corresponded to the correct task (matching colored bands and squares), except for eye movements.

Figure 5: Decoding z-score (FDR-corrected, $q=0.05$) during long task RUN2 for all subjects and movement types. The colored bands correspond to the periods of the tasked stimuli and the lines indicate the decoding scores. The colors corresponding to movement types displayed in the legend. Peaks of the decoding z-score are denoted with squares in respective colors. The movement type with the highest decoding score generally corresponded to visual-cued movement condition (matching colored bands and squares), except for eye movements.

Figure 6: Decoding z-score (FDR-corrected, $q=0.05$) for all movement types during 5 minutes resting state for Subject 1 to 7. Spatial maps showing SPFM activations in z-score (red-yellow) overlay on meta-maps for time frames for $n=7, 59, 88, 116$, and 195 for Subject 1 are also shown at the top of the figure. The colored bands indicate movement detected in EMG traces with the movement type shown by the color in the legend. The colored lines show the decoding z-scores for each meta-map type. The movement type with the highest decoding z-score is indicated by a colored square. Asterisk (*) denotes decoded events that coincided with movements detected on EMG traces.

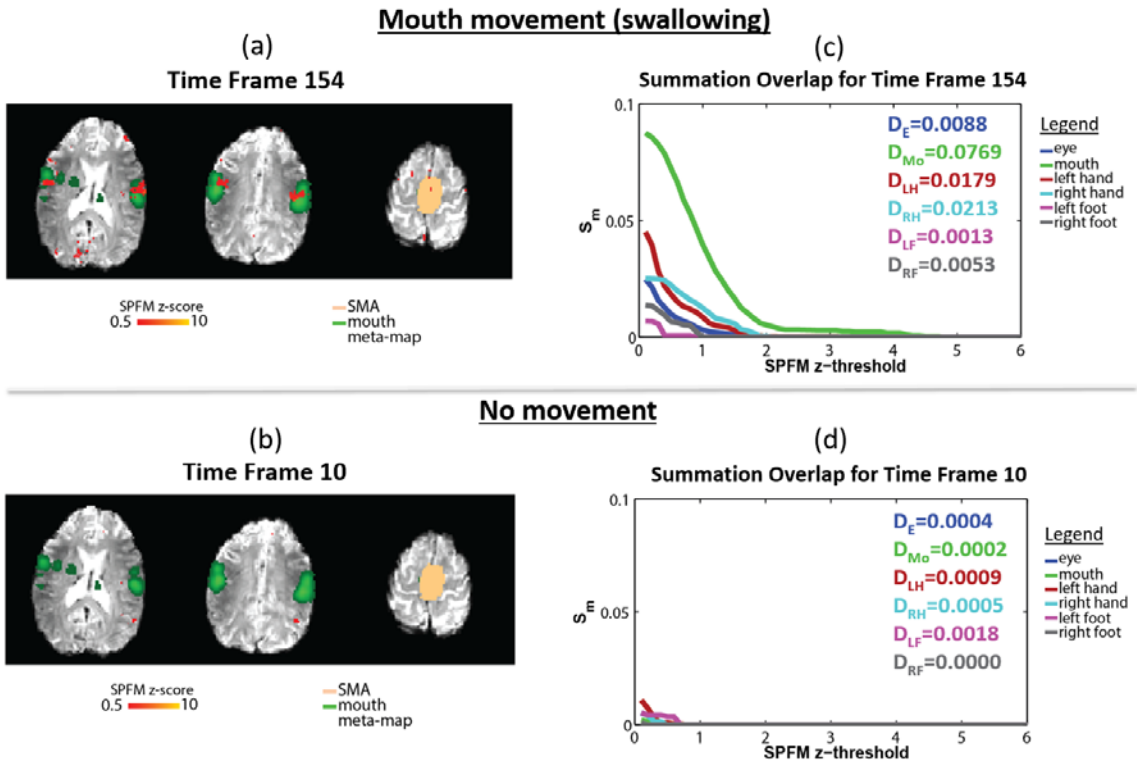
867 Figure 1



868

869

870

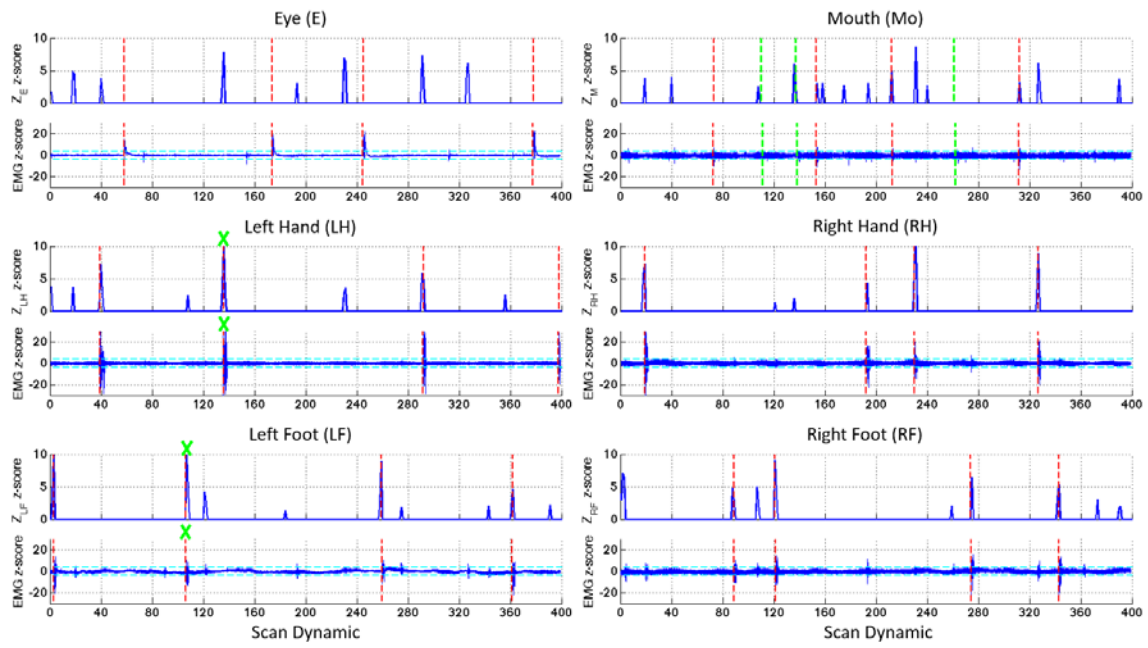


872

873

874

875 Figure 3

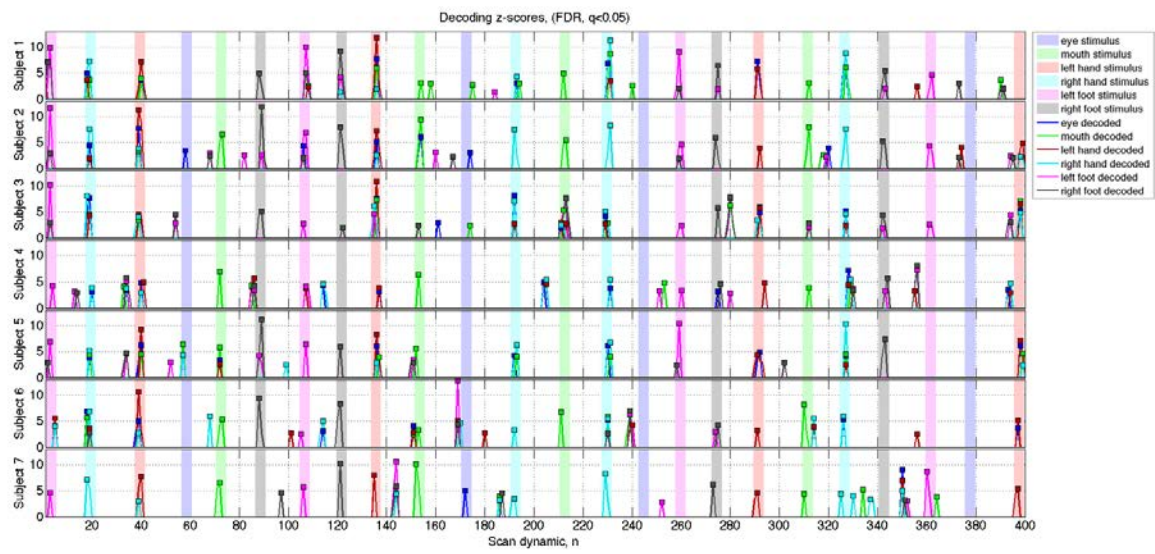


876

877

878

879 Figure 4

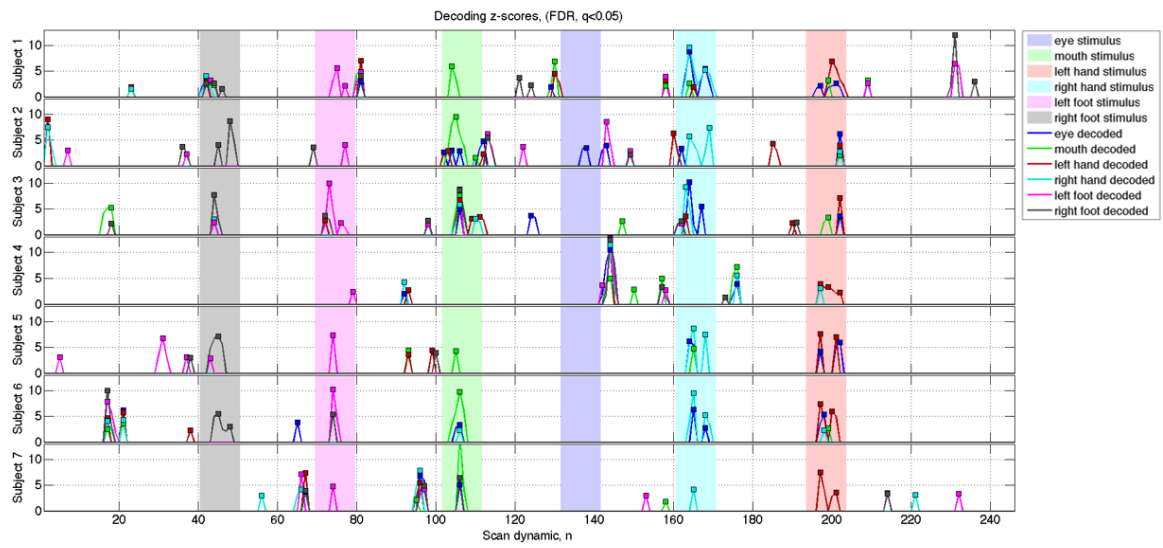


880

881

882

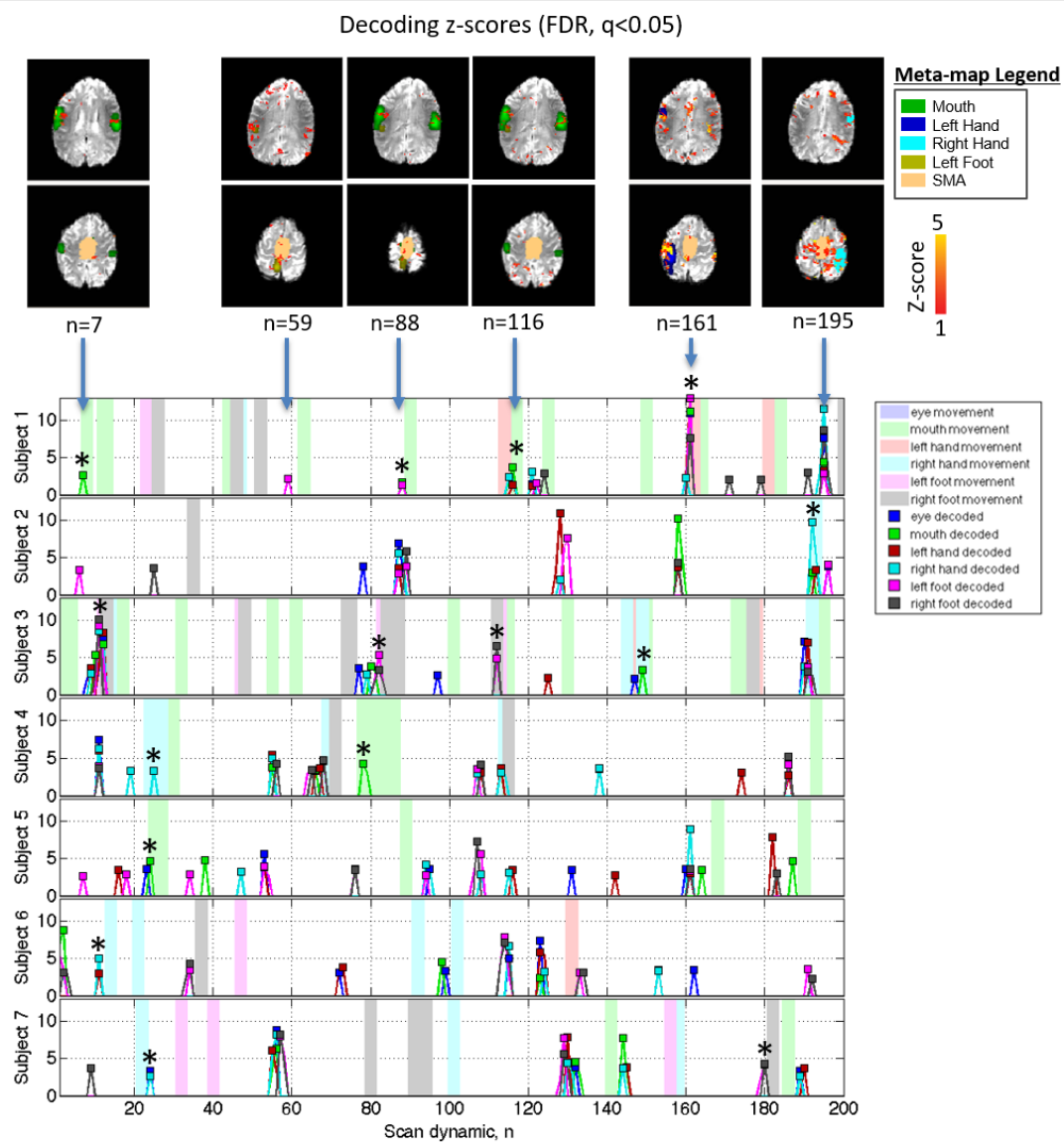
883 Figure 5



884

885

886



888
889
890

Table I: Details on meta-map for each of the six movement tasks: eye (E), mouth (M), left and right hand (LH and RH), and left and right foot (LF and RF). The number of studies used to form each meta-map is listed, together with the total number of significant ALE voxels, and maximum and minimum ALE range in each meta-map.

<div> </div>						
Movement Type	Eye (E)	Mouth (Mo)	Left Hand (LH)	Right Hand (RH)	Left Foot (LF)	Right Foot (RF)
No. of studies	24	18	21		14	
No. of significant ALE voxels	6208	6411	3870	3877	2014	2012
Maximum ALE (at centre of cluster)	0.063	0.050	0.054	0.005	0.046	0.044
Min ALE	$1.7 \cdot 10^{-8}$	$1.5 \cdot 10^{-9}$	$4.0 \cdot 10^{-10}$	$3.3 \cdot 10^{-9}$	$3.7 \cdot 10^{-9}$	$3.7 \cdot 10^{-9}$

897 **Table II:** Percentage overlap between meta-maps calculated as the overlap area divided by the
898 number of voxels in region (b). The SMA was excluded from all calculations.

		PERCENTAGE OVERLAP BETWEEN META-MAPS, $[(a) \cap (b)] / (b)$				
(a) \ (b)	Eye	Mouth	Left Hand	Right Hand	Left Foot	Right Foot
Eye	100.0	11.3	11.4	10.4	0.0	0.0
Mouth	8.9	100.0	7.2	7.0	1.2	1.3
Left Hand	17.7	14.2	100.0	0.0	2.1	0.0
Right Hand	15.4	13.3	0.0	100.0	0.0	4.2
Left Foot	0.0	6.3	5.6	0.0	100.0	8.6
Right Foot	0.0	5.9	0.0	10.2	7.4	100.0

899

900

901 **Table III:** Summarizing the classification of different events for the example of hand movements.

	No movement decoded in area expected from task or EMG	Movement decoded in area expected from task or EMG
EMG: No movement	Potential True Negative (pTN): Cannot be sure since EMG only monitors certain muscle locations	Potential False Positive (pFP): Cannot be sure since EMG only monitors certain muscle locations
EMG: Movement	False Negative: Decoding method either did not predict an event (FN_{null}), or decoded it incorrectly (FN_{wron})	True Positive (TP)

902

Table IV: Events decoded in short movement task (RUN1). (a) Number of events where the highest decoding z-score rank corresponded with the visually-cued tasked movement and EMG, (*except Subject 4, where validation was used visually-cued tasked movement only for left and right foot). (b) Total number of false negatives due to a misclassification (FN_{wrong}) or no event detected (FN_{null}). (c) Success rate of decoded events averaged over all movement types, which describes the sensitivity of the decoding method. An event is successfully decoded when its highest rank of meta-map channel matches the visually-cued tasked movement and is confirmed by EMG. (d) Number of decoded events which were not associated with stimuli or EMG traces (potential false positives). (e) Total null regressors (time frames that had more than 0.5mm/scan displacement) that were included in the SPFM analysis. For subject 2, time frames n=203 to 208, which were during periods of rests, were also excluded due to artefacts.

SHORT TASK PARADIGM (TASK-BASED MOVEMENTS)										
Subject	(a) Number of events detected by decoding as a fraction of number expected by task and confirmed by EMG						Excluding eye movements			(e) Total Null Regressors
	Eye	Mouth	Left Foot	Right Foot	Left Hand	Right Hand	(b) Total False Negative (FN _{wrong} FN _{null})	(c) % decoded task events (sensitivity)	(d) Number of decoded events not associated with stimuli or EMG (pFP)	
1	0/4	3/4	4/4	4/4	2/4	4/4	3(1 2)	85	5	0
2	2/4	4/4	4/4	4/4	4/4	4/4	0	100	5	5
3	0/4	0/4	4/4	4/4	1/4	2/4	9(8 1)	55	4	15
4	0/4	3/4	3/4*	2/4*	4/4	2/4	6(2 4)	70	8	5
5	0/4	2/4	3/4	3/4	3/4	4/4	5(1 4)	75	7	0
6	0/4	4/4	1/3	3/4	3/3	3/4	4(2 2)	77	0	10
7	1/4	3/4	3/4	2/4	4/4	4/4	4(0 4)	80	5	5
Total False Negative (FN _{wrong} FN _{null})	25 (0 25)	9 (3 6)	6 (1 5)	6 (0 6)	6 (4 2)	5 (4 1)				
% success rate average d over all subjects	11	68	77	82	79	82				

Table V: Spontaneous (non-task) events were decoded in the short movement task (RUN1) (highest ranked decoding z-score Z_m corresponds with correct spontaneous movement type in EMG trace). This table shows the number of events successfully decoded out of total number of events detected via EMG, excluding eye movements, and provides the best estimate of sensitivity for spontaneous events.

Subject	Number of successfully decoded events as a fraction of number of events detected via EMG (excluding eye movements)
1	0/3
2	0/3
3	4/17 (1 mouth, 3 Right Foot)
4	1/13 (1 mouth)
5	0/1
6	0/3
7	0/2

Table VI: Events decoded in long movement task (RUN2). (a) Number of events successfully decoded in long task paradigm, which was verified using both stimuli markers and EMG. The expected total number of tasks perform per movement type is 1. (b) Total number of false negatives due to a misclassification (FN_{wrong}) or no event detected (FN_{null}). (c) Success rate of decoded events excluding eye movements (sensitivity). (d) Number of decoded events which were not associated with stimuli or EMG traces (potential false positives). (e) Total null regressors (time frames that had more than 0.5mm/scan displacement) that were included in the SPFM analysis. *For subject 1, 10 time frames were manually excluded from analysis due to residue artefact detected upon visual inspection (scan dynamic=24 to 27, 58 to 65). These time frames occurred during rest periods.

LONG TASK PARADIGM										
Subject	(a) Number of events decoded as a fraction of number expected by task and confirmed by EMG						Excluding eye movements			(e) Total Null Regressors
	Eye	Mouth	Left Foot	Right Foot	Left Hand	Right Hand	(b) Total False Negative (FN_{wrong} FN_{null})	(c) % decoded task events (sensitivity)	(d) Number of decoded events not associated with stimuli or EMG (pFP)	
1	0/1	1/1	1/1	0/1	1/1	1/1	1(1 0)	80	5	11*
2	0/1	1/1	1/1	1/1	0/1	1/1	1(1 0)	80	9	10
3	0/1	0/1	1/1	1/1	1/1	0/1	2(2 0)	60	6	9
4	0/1	0/1	1/1	0/1	1/1	0/1	3(0 3)	40	3	23
5	0/1	0/1	1/1	1/1	1/1	1/1	1(0 1)	80	3	0
6	0/1	1/1	1/1	1/1	1/1	1/1	0	100	1	0
7	0/1	1/1	1/1	0/1	1/1	1/1	1(0 1)	80	5	0
Total False Negative (FN_{wrong} FN_{null})	7 (0 7)	3 (1 2)	0	3 (1 2)	1 (1 0)	2 (1 1)				
% success rate average d over all subjects	0	57	100	57	86	71				

Table VII: Events decoded in resting state (RUN1). (a) Number of successfully decoded events (highest ranked Z_m correspond with correct movement type in EMG trace) divided by the total number of movements detected in EMG. (b) Number of decoded spontaneous events which were not associated with stimuli or EMG traces. Eye movements were excluded for all tabulations. (c) Total null regressors (time frames that had more than 0.5mm/scan displacement) that were included in the SPFM analysis. *For subject 7, 6 time frames were manually excluded from analysis due to residue artefact detected upon visual inspection (scan dynamic, $n = 49$ to 54).

MOVEMENTS DURING RESTING STATE (excluding eye movements)			
Subject	(a) Number of spontaneous movements decoded and confirmed by EMG as a fraction of number expected by EMG	(b) Number of decoded events not associated with EMG trace	(c) Total Null Regressors
1	4/19 (3 mouth, 1 left hand)	8	9
2	1/2 (1 right hand)	5	0
3	4/32 (2 right foot, 1 left foot, 1 mouth)	1	0
4	2/12 (1 right hand, 1 mouth)	8	0
5	1/4 (1 mouth)	9	0
6	1/7 (1 right hand)	7	5
7	2/12 (1 right foot, 1 right hand)	3	0 *